Micrometeorite bombardment simulated by ns-pulsed laser ablation: Morphological characterization of the impact craters

Daniele Fulvio[1,2]*, Leonardo Fuks Maron[1], Yaima Cires Perez[1], Tahir[1], and Tommaso Del Rosso[1]

[1]Department of Physics, Pontifícia Universidade Católica do Rio de Janeiro, Rua Marques de São Vicente, 22451- 900, Rio de Janeiro, Brazil

[2]Present Address: Istituto Nazionale di Astrofisica, Osservatorio Astronomico di Capodimonte, Salita Moiariello 16, 80131, Naples, Italy

Corresponding author: daniele.fulvio@inaf.it;

Abstract

The term “space weathering” refers to processes that include changes in the physical, chemical, mineralogical, and spectral properties of the surface of asteroids, comets, and some planets and their satellites, such as the bombardment by micrometeorites, solar wind ions, and cosmic rays. In this study, we focus on micrometeorite impacts, which may be the primary contributor to the annual mass flow of material that reaches the surface of such bodies. Studying the processes and effects

associated with micrometeorite impacts is fundamental for understanding the evolution of the solar system and its components. From an experimental point of view, it is typically assumed that micrometeorite impacts may be simulated by ns-pulsed lasers and, indeed, many experimental studies have been performed based on such assumption. These studies have the common main goal to understand how micrometeorite impacts may change the physical-chemical and spectral properties of the bombarded surfaces. However, here we perform the first experimental study dedicated to the morphological characterization of the impact craters created by ns-pulsed laser ablation, in order to determine how well ns-pulsed lasers simulate the crater morphology of natural micrometeorite impacts. For this purpose, the laser ablation technique was applied to three different silicates: feldspar, quartz, and jadeite. For each of these minerals, two ablation scenarios have been considered: in air and in water. The craters formed by ns-pulsed laser ablation were characterized, from the morphological point of view, using a profilometer. Using this data we estimated the depth:diameter ratio of each crater. The comparison with literature data shows that the simple craters formed by ns-pulsed laser ablation closely resemble craters formed by natural micrometeorite impacts. In other words, from a morphological point of view, ns-pulsed laser ablation is appropriate for the simulation of micrometeorite impacts. We additionally verified that the value of the depth:diameter ratio does not depend, within errors, on the total number of laser pulses or the repetition frequency, at least within the ranges covered in these experiments: i) between 1 and 1200 laser pulses and ii) between 1 and 10 Hz.

Keywords: micrometeorite; laser ablation; impact crater; space weathering; laboratory astrophysics;

1. Introduction

In the solar system, the surfaces of airless planetary bodies like asteroids, comets, and some planets and their satellites are constantly exposed to the space environment and, as a result, the physical, chemical, and spectral properties of these surfaces are gradually altered. The term "space weathering" refers to the processes inducing these changes, such as bombardment by micrometeorites, solar wind ions, and cosmic rays. Investigating the processes and mechanisms associated with space weathering is necessary to comprehensively understand solar system evolution (e.g., Hapke 2001; Sasaki et al., 2001; Clark et al., 2002; Chapman 2004; Brunetto et al., 2006, 2015; Gaffey et al. 2010; Matsuoka et al., 2015; Fulvio et al. 2016, 2018; Greer et al. 2020; Kohout et al. 2020; Weber et al. 2020). Space weathering is responsible for the spectral mismatch between the visible (Vis) to near-infrared (NIR) reflectance spectra of the lunar samples returned by the Apollo missions and the lunar soil. Similarly, space weathering is also responsible for the Vis-NIR spectral mismatch between the spectra of the ordinary chondrite meteorites and their parent bodies, the S-type asteroids (e.g., Cassidy and Hapke 1975; Pieters et al. 2000; Brunetto and Strazzulla 2005; Loeffler et al. 2008, 2009; Pieters and Noble 2016). Laboratory space weathering simulations performed on lunar samples and ordinary chondrites showed that space weathering processes change the Vis-NIR spectral properties of the bombarded surface, causing progressive spectral darkening (i.e. decreasing albedo), reddening (i.e. variation of the spectra slope, with lower reflectance at lower wavelength), and weakening of absorption bands. From a physical-chemical point of view, space weathering produces coatings of nanophase metallic iron ($npFe^0$) on the bombarded surface. These coatings may be produced by re-deposition of iron sputtered by solar wind and cosmic ions and/or re-

deposition of iron-containing vapors produced by micrometeorite impacts. Direct confirmation of these effects of space weathering has been recently provided by analyzing the samples returned from asteroid 25143 Itokawa by the JAXA Hayabusa space mission (see e.g. Noguchi et al. 2014; Matsumoto et al. 2016, 2020). A more detailed discussion including the space weathering effects on the Moon, S-type asteroids, and other airless planetary bodies goes beyond the scope of this study and we refer the interested reader to the references given above. As previously mentioned, space weathering processes can be grouped into two main categories, related to: (a) impacts by micrometeorites and (b) irradiation by ions, photons, or electrons. In this study, we focus on the first **phenomenon**: micrometeorite impacts that occur on airless bodies of the solar system.

Since Earth has an atmosphere, its surface is unaffected by space weathering processes. However, it is interesting to note that based on the material collected by the NASA Long Duration Exposure Facility spacecraft (Love and Brownlee 1993), the total mass of micrometeorites reaching Earth' surface is estimated to be about 4×10^7 kg / year (the mass range was 10^{-9} to 10^{-4} g). This represents a significant amount of the flux of extraterrestrial mass when compared to the total mass of meteorites (mass > 10^{-1} g) reaching the surface, estimated (by using earth-based and satellite measurements) at about 5×10^4 kg / year (Zolensky et al., 2006). With this example we want to simply point out that, like in the case of Earth, micrometeorites may largely contribute to the annual mass flow of material that reaches the surface of asteroids, comets, and some planets and their satellites. Additional details on the mass flow of material that reaches the surface of some of these objects can be found in the recent paper by Plane et al. (2018) and references therein. In the specific case of the Moon, the reader may also want to refer to Grün et al. 1985 and Vanzani et al. 1997. With that being said, it is

evident that studying the physical, chemical, morphological, and spectral effects of micrometeorite bombardment on airless planetary surfaces is fundamental to understanding the evolution of the solar system and its components.

Micrometeoroids in space have a mean velocity ranging from a few to several tens of km/s (Plane et al. 2018). From an experimental point of view, it is difficult to recreate micrometeorite bombardment through hypervelocity impacts in the laboratory. To the best of our knowledge, only a few laboratories around the world have facilities capable of performing such experiments (e.g., Cintala et al. 1999; Shu et al. 2012; Thomas et al. 2016, 2017; Barnouin et al. 2019). Aware of this, an alternative experimental method emerged **a** few decades ago to obtain comparable results and to better understand the physics behind the formation of impact craters: laser irradiation. The key aspect of this method is to simulate the impact of micrometeorites using a nanosecond (ns) pulsed laser. This technique, generally known as "pulsed laser ablation", **has** several applications in modern technology and **has been** employed in many research areas, such as the precise micromachining of materials and the production of different **kinds** of nanostructures and thin films (e.g., Cheung and Horwitz 1992; Radziemski 1994; Liu et al. 1997; Babushok et al. 2006; Ganeev et al. 2007; Amendola and Meneghetti 2013; Del Rosso et al. 2016, 2018).

Although the use of a **lasers** to simulate **micrometeorite** bombardment is not intuitive, laser ablation is an indirect technique through which similar physical-chemical processes are induced in the bombarded sample, as theoretically described already by Yurij and Vekhov (1979) and Kissel and Krueger (1987). **Like micrometeorite impacts**, laser pulses cause a prompt release of energy within the sample, **resulting in** ablation (removal) of **some sample material**. Pulsed laser ablation processes are based on the absorption of the energy of the short laser pulse by the electrons of the surface of

125 the target, followed by phonon thermalization in times of the orders of ps (Perez and
126 Lewis 2003). The mechanism related to the ejection of the material strongly depends on
127 the length of the laser pulses. While ultrashort pulses (fs, ps) mostly lead to multi-
128 photon absorption processes and photo-ionization effect with Coulombic explosion and
129 explosive boiling (Perez and Lewis 2003; Hashida et al. 2009), pulsed laser ablation by
130 the use of ns or longer pulses is instead dominated by thermal processes, such as
131 melting and vaporization of the material (Jaeggi et al. 2011; Gusarov and Smurov
132 2005). The material removed from the target by pulsed laser ablation is finally
133 transformed **into** nanoparticles whose size and chemical composition depend in a
134 complex way on both the nature of the ablated material, the laser-pulse characteristics,
135 and the nature and composition of the external environment (Scharf and Krebs 2002;
136 Giorgetti et al. 2007; Amendola and Meneghetti 2013; Del Rosso et al. 2016, 2018;
137 Araujo et al. 2020).

138 Compared to natural micrometeorite impacts, ns-pulsed lasers successfully
139 simulate: (1) the duration of the vaporization process induced by micrometeorite
140 impacts; (2) the timescale of the process of energy deposition into the target (Yurij and
141 Vekhov 1979; Kissel and Krueger, 1987; Yamada et al., 1999; Brunetto et al., 2006;
142 Loeffler et al., 2008; Matsuoka et al., 2015; Wu et al., 2017). Another fundamental
143 aspect of micrometeorite impacts that must be successfully simulated is the total energy
144 deposited into the target material. While the aforementioned similarities have made ns-
145 pulsed lasers one of the best experimental approaches for simulating natural
146 micrometeorite impacts, **there could be** limitations to this method, **specifically**
147 concerning **its failure to reproduce the** deformation effects observed in natural
148 **micrometeorite** impact craters, such as dislocations, shock vitrification, and fracturing
149 (Christoffersen et al. 2016; Noble et al. 2016).

Beginning in the 1990s, laser irradiation experiments were routinely used to simulate micrometeorite impacts on the surfaces of airless bodies in the solar system, **however, a standardized laser irradiation setup was not established**. In this context, Moroz et al. (1996) and Wasson et al. (1998) irradiated olivines, clinopyroxenes, ordinary chondrites and HED (Howardite, Eucrite and Diogenite) meteorite samples with microsecond pulsed lasers to study the so-induced changes in their reflectance spectra. To better simulate the impact physics of micrometeorite bombardment processes, Yamada et al. (1999) and Sasaki et al. (2001, 2002) used ns-pulsed lasers. In these experiments, the olivine and pyroxene samples were irradiated by a pulsed laser beam with **a** wavelength of 1064 nm **and** pulse duration **of** 6-8 ns. Brunetto et al. (2006) also simulated the effects of micrometeorite bombardment using a ns pulsed laser, with pulse of 20 ns, at two different wavelengths, 193 and 248 nm. A few years later, Loeffler et al. (2008) used a laser of 193 nm with pulses of 10 ns on olivine and forsterite samples to examine the spectral effects **resulting from impact vapor and melt re-deposition**. Being this topic of great interest in planetary science, many more recent studies have focused on the effects of space weathering using ns-pulsed laser irradiation of meteorites and terrestrial analogues, e.g., Matsuoka et al., 2015, 2020 (laser irradiation of the carbonaceous chondrite Murchison, 6-8 ns pulse duration, wavelength of 1064 nm), Wu et al., 2017 (irradiation of a terrestrial basalt, anorthosite, an ordinary chondrite type H and an iron meteorite; pulsed laser of 6 ns and wavelength of 532 nm), Gillis-Davis et al., 2017 and Kaluna et al. 2017 (laser irradiation of the carbonaceous chondrite Allende and of Fe- and Mg-rich aqueously altered minerals; 6 ns pulse duration and wavelength of 1064 nm), Thompson et al., 2019, 2020 and Prince et al., 2020 (laser irradiation of the carbonaceous chondrite Murchison and of troilite samples; 6-8 ns pulse duration and wavelength of 1064 nm).

All these experimental studies have a common main goal: understanding how micrometeorite bombardment may change the physical, chemical, mineralogical, and spectral properties of the surfaces of airless bodies of the solar system. Although many interesting results have been obtained, there is no experimental study, to the best of our knowledge, dedicated to the morphological characterization of the impact craters created by ns-pulsed laser ablation and, as a consequence, to understanding the suitability of pulsed laser ablation as a technique for simulating micrometeorite impacts. A mismatch between the morphology of craters created by ns-pulsed laser ablation and natural micrometeorite bombardment would imply that our comprehension about the physical processes occurring during the impacts is just partial and still needs to be improved. On the contrary, a good match would suggest that ns-pulsed lasers are indeed one of the best experimental approaches for simulating natural impacts. In this study we help address this outstanding question by performing the first morphological characterization of craters created by ns-pulsed laser ablation.

We irradiated three different silicate samples (feldspar, quartz, and jadeite) to investigate how well ns-pulsed lasers simulate the crater morphology of natural micrometeorite impacts. For each silicate, we considered two ablation scenarios: in air and in water. This was done to determine if the morphological characteristics of the impact craters depend (keeping all others laser parameters fixed) on the external medium within which the mineral is impacted. The experiments performed in water aim to simulate those astrophysical cases where liquid water may be present, even just transiently, on the surfaces of asteroids, comets, and some planets and their satellites. We point out that results from the laser ablation experiments performed in water may also be relevant to icy planetary bodies since, upon micrometeorite impact, the ice along the impact track would immediately melt. It is evident that to have an actual impact

with the underlaying surface, the penetration depth of the micrometeoroid needs to be higher than the thickness of the overlayer of water. If this is not the case the micrometeoroid will simply implant into the covering layer without reaching the minerals on the surface.

More caution should be taken when considering that the experiments have been performed in air, i.e. ambient pressure. Strictly speaking, they should have been performed under vacuum as to better simulate the pressure conditions encountered in space. This was not possible in our experimental setup and, to the best of our knowledge, there are no studies comparing the effects of ns-pulsed laser ablation in air and in vacuum. However, several studies exist that compare the effects of fs-pulsed laser ablation of various targets in air versus vacuum environments. Taking into due account the differences with our experimental setup (mainly, the pulse duration), these studies indicate that the effects of laser ablation in air and in vacuum are comparable when considering low/moderate laser fluence regimes which is the case of the experimental setup used in the current study. In these works the ablation of fused silica and Al-Mg alloy were studied, in air and vacuum, by using fs-pulsed lasers (wavelength: 800 nm; pulse width: 35 fs; repetition rate: 10-100 Hz) with pulse fluences up to 41 J/cm^2. Among the main results, it is shown that the morphology of the craters and the consequent similarities/discrepancies in air and vacuum depend on three ablation regimes: low, moderate, and high. At low/moderate laser fluences, in air and vacuum there are no striking differences while in the high fluence regime there are. The starting of the high fluence regime depends on the ablated material. As an example, in the case of fused silica the high fluence regime starts at about 9.5 J/cm^2. For fluences higher than 9.5 J/cm^2 the crater diameter is larger and its depth smaller in air than in vacuum (Xu et al. 2016). Similarly, in the case of Al-Mg alloy the high fluence regime

starts at about 4.5 J/cm^2 (Dou et al. 2018). Additional details can be found in Xu et al. 2016; Dou et al. 2018 and references therein.

2. Material and Methods

2.1 Preparation of the mineral samples

In this study, we simulated micrometeorite impacts on the surfaces of airless bodies by subjecting feldspar, jadeite, and quartz mineral samples to ns-pulsed laser irradiation. **These samples were** part of a collection of minerals donated to the Van der Graaf Laboratory at the Physics Dept. of PUC-Rio University and were **compositionally** characterized by the Brazilian Agency Companhia de Pesquisa de Recursos Minerais. As silicates, these target minerals contain mainly silicon (Si) and oxygen (O) in their **crystal structure**. The chemical formula of common feldspars can be expressed in terms of three end members: $KAlSi_3O_8$, $NaAlSi_3O_8$ and $CaAl_2Si_2O_8$. Solid solutions of these end members also exist in nature. The average density of feldspars is 2.55 – 2.75 g/cm^3. Jadeite belongs to the pyroxene family and its chemical formula is $NaAlSi_2O_6$. Its average density is of about 3.34 g/cm^3. Quartz is a mineral composed of silicon and oxygen atoms, giving an overall chemical formula of SiO_2. Its average density is about 2.65 g/cm^3. Iron (Fe) should not be present in feldspar, jadeite, or quartz, however, depending on the conditions under which the mineral crystallized, Fe can be a trace/contaminant element in their structure. For example, elemental analysis of jadeite samples reported in the literature show a typical total iron content below 0.6 wt% (e.g., Rossman 1974; Nassau and Shigley 1987; Shinno and Oba 1993; Harlow and Shi 2011). Based on these literature data, the total amount of Fe in jadeite samples (those where iron has been detected) would typically be at least 40-60 times

less than the total amount of Al, up to reaching the ideal case of those jadeite samples where there has been no detection of iron. A similar discussion **exists** for feldspars (e.g., Hofmeister and Rossman 1984; Polyak et al. 1999; Dyar et al. 2001). Unfortunately, we cannot provide a more specific formula for the composition of our feldspar sample. Considering our work focuses on crater morphology (i.e., ultimately, the physical properties of the irradiated sample) rather than the chemical and/or mineralogical effects induced by pulsed laser irradiation, to first approximation, this lack of feldspar compositional data should not impede our analyses or conclusions. In fact, it is well known that feldspar minerals share various physical properties that are remarkably coherent (e.g., Lide, 2004 and https://geology.com/minerals/feldspar.shtml). A more detailed classification and description of these minerals goes beyond the scope of this paper.

Feldspar, jadeite, and quartz are minerals of extreme interest in the field of planetary science since they are found in terrestrial and extraterrestrial rocks (e.g., Rudnick and Gao 2003; Norton and Chitwood 2008; Anderson and Anderson, 2010; Bockelée-Morvan et al. 2017; Komatsu et al. 2018; Ootsubo et al. 2020). As an example of their extraterrestrial occurrence, feldspar was identified in lunar rocks and martian and HED meteorites (Szurgot 2014; Hill 2016; Cassata et al. 2018; Zhang et al. 2020). Similarly, jadeite was found in some samples of ordinary chondrites (e.g., Ozawa et al. 2014; Ohtani et al., 2017 and references therein) and carbonaceous chondrites (Miyahara et al., 2015). Moreover, tissintite (the Ca-bearing isostructural phase of jadeite) recently was identified in the martian meteorite Tissint and the eucrite Northwest Africa (NWA) 8003 (Ma et al. 2015; Pang et al. 2016). Finally, quartz (and other silica polymorphs) was found in heavily shocked meteorites (e.g., Kimura et al. 2005; Tomioka and Miyahara 2017).

Samples of the aforementioned minerals were prepared according to the following procedure. The raw minerals, in pieces, were subjected to three cycles of ultrasonic cleaning in acetone for 30 minutes each, in order to remove potential impurities. Each mineral was then crushed into a powder using an agate mortar and pestle and subsequently pressed onto an indium support to create pellets for the experimental procedure (the grain size of the powdered samples was below 100 μm). For each pellet 0.1 g of mineral powder and 1.0 g of indium were used. A support was necessary since without it the silicate pellet would be fragile and easily broken. Indium was chosen since it is a soft metal, easy to manipulate, and it is not present in the silicate samples studied. The sample preparation procedure was always the same: the indium support was prepared by pressing 1.0 g of indium to 0.2 ton cm^{-2} for 1 minute in a hydraulic press. Subsequently, the silicate pellets were obtained by pressing 0.1 g of the selected mineral on the previously prepared indium support, to 1 ton cm^{-2} for 6 minutes. Following this procedure, four pellets (13 mm in diameter) for each of the three silicates (feldspar, quartz and jadeite) were prepared, yielding a total of twelve.

Before performing the laser ablation experiments, each freshly-made pellet was inspected for potential surface heterogeneities caused by sample preparation using a Zeiss AX10 optical microscope. No craters were observed in any of the pellets at this stage. Two ablation experiments were performed with each silicate, to simulate two distinct experimental scenarios: one ablation with the silicate pellet in ambient air and one with it immersed in deionized water. In addition, to increase the number of experimental data, two laser fluences ($\boldsymbol{F_{pulse}}$) were considered for each mineral, except for quartz (only one fluence in this case because of a problem with the laser setup during the experimental run). This way, ten of the twelve pellets were used and a total of ten craters were created. All experiments were performed at room temperature.

2.2 Laser ablation experiments

To simulate the crater formation process induced by micrometeorite impacts we used ns-pulsed laser ablation. The system used was a Nd:YAG laser (Quantel U.S.A, model BIG SKY), with pulse duration of 8 ns, operating simultaneously at the wavelengths λ_1 = 532 nm (frequency 2ω) and λ_2 = 1064 nm (frequency ω), with a nominal diameter of the pulse at the exit of the laser equal to 2.5 mm. During the ablation, we did not scan laser pulses across the target surface, resulting in a single crater per experiment. The laser pulses are reflected by a BK7 prism which deviates them perpendicularly to the sample/external medium interface (air or water). The laser pulses are focused on the target by a BK7 lens with a focal distance of about 14 cm, and the pulse fluence $F_{pulse} = F_{\omega} + F_{2\omega}$ (with F_{ω} and $F_{2\omega}$ corresponding to the fluence of the pulses at the ω and 2ω frequency, respectively) is controlled by adjusting both the energy of the laser pulse and the lens-target distance (see Figure 1). The energy of the laser pulses at both the fundamental and second harmonic wavelength was measured using a pyroelectric detector from ThorLabs (model ES220C, USA). The target-lens distance was properly adjusted in order to ensure that the pulses impinging on the surface of the target at the ω and 2ω frequency had approximatively the same fluence ***F***. The procedure followed for the determination of the fluences at ω and 2ω frequencies both in air and water environment, is described in detail in the Supplementary Material. In our system, the energy of the laser pulses $E_{pulse} = E_{\omega} + E_{2\omega}$ ranges from 3 to 6 mJ. These values are comparable with energies of micrometeorites with mass below 10^{-8} - 10^{-9} kg and with diameter of few microns (e.g., Zolensky et al. 2006). The main

characteristics of the single laser pulse (E, F, diameter on the target ϕ) at both ω and 2ω frequency are reported in Table 1. If not otherwise specified, the laser source repetition frequency was kept equal to 10 Hz and each sample was irradiated for a total time of 120 s, resulting in 1200 pulses total per ablation experiment and receiving a total amount of energy $\boldsymbol{E_{total}}$. **We also** performed additional laser irradiation experiments on one jadeite sample in air (irradiating each time a different spot of its surface) to compare the craters formed with 1, 10, 100 and 1200 total pulses, keeping fixed E_{pulse} = 6 mJ and F_{pulse} = 4.2 J/cm^2. **All these experiments are discussed in Section 3**. Finally, we point out that in the experiments with the target immersed in H_2O the pellets were stable (i.e., did not show signs of sample separation, floating or falling apart) and the height of the liquid was kept at 3 mm above the upper surface of the target, in order to minimize the focusing effect of water.

It is important to understand that the depth and diameter of craters formed by pulsed laser ablation are influenced by the fluence threshold (e.g., Jaeggi et al. 2011; Zheng et al. 2014). The fluence threshold (F_{th}) is the minimum fluence needed to ablate a target material, and this value depends on the target material composition and the pulse duration and wavelength used in the irradiation experiments. Consequently, in morphological studies (such as the present one), crater depths and diameters are influenced strongly by the pulse duration and wavelength of the incident laser. In particular, we point out that the diameter of craters produced by ns-pulsed laser ablation can be either smaller or bigger than the spot size of the laser pulse on the target (ϕ_ω and $\phi_{2\omega}$ in Table 1). This effect depends essentially on the natural logarithmic function of the ratio between the working fluence and the threshold fluence at the wavelength of interest, for each specific material (e.g., Cabalin and Laserna 1998; Sikora et al. 2017). While the choice of the ns-pulse duration has been already discussed

in the Introduction, there is no direct association between the physical properties of micrometeorites (such as its velocity or mean size) and a particular wavelength of the laser pulse. In this view, the use of a specific wavelength rather than another would lead to an intrinsic bias, which can be overcome by the simultaneous irradiation with pulses of different wavelengths. For this reason, our laser ablation experiments simultaneously irradiate silicate targets with both an infrared- and visible-wavelength laser pulse. Two parameters mainly rule the dimension of the crater after the interaction with the laser pulse: i) the diameter of the laser pulse spot on the target, and ii) the threshold fluence F_{th}. A bigger diameter of the laser beam will lead to a bigger linear dimension of the crater, while a bigger value of F_{th} will lead to a smaller linear dimension (Sikora et al. 2017). Since the infrared laser pulses have a higher value of F_{th} compared to the case of visible pulses, we expect that when $F_{\omega} \approx F_{2\omega}$, bigger diameters and depths of the craters should be obtained when using the 2ω pulses. On the other hand, in our configuration, the diameter of the 2ω pulses at the surface of the target is relatively smaller than the diameter of the ω pulses (see Table 1), coherently with the well-known dependence of the diffraction limited beams on the wavelength of electromagnetic waves (e.g., Born and Wolf, 1999). Diffraction hence compensate, in first approximation, the effect due to the different values of F_{th}.

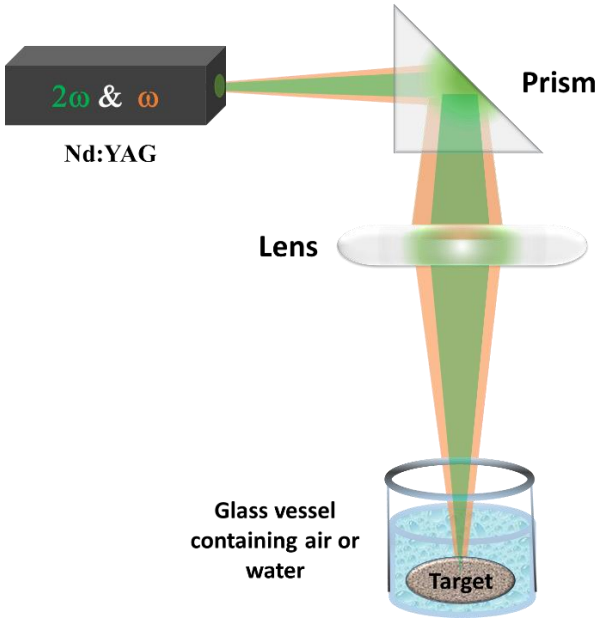

Figure 1: Schematic of the laser ablation setup used in the experiments to simulate the micrometeorite impacts. The laser source simultaneously emits pulses at both ω and 2ω frequency (see main text for the details).

Energies and Fluencies used in the experiments							
Exp. Scenario #1: air							
Mineral	F_{pulse} **(J/cm²)**	F_{ω} **(J/cm²)**	$F_{2\omega}$ **(J/cm²)**	E_{pulse} **(mJ)**	E_{ω} **(mJ)**	$E_{2\omega}$ **(mJ)**	E_{total} **(J)**
jadeite	2.7	1.4	1.3	3.9	2.5	1.4	4.7
jadeite	4.2	2.2	2.0	6.0	3.8	2.2	7.2
quartz	4.2	2.2	2.0	6.0	3.8	2.2	7.2
feldspar	3.8	2.0	1.8	5.4	3.4	2.0	6.5
feldspar	4.2	2.2	2.0	6.0	3.8	2.2	7.2
Exp. Scenario #2: water							
Mineral	F_{pulse} **(J/cm²)**	F_{ω} **(J/cm²)**	$F_{2\omega}$ **(J/cm²)**	E_{pulse} **(mJ)**	E_{ω} **(mJ)**	$E_{2\omega}$ **(mJ)**	E_{total} **(J)**
jadeite	2.3	1.2	1.1	3.3	2.1	1.2	4.0
jadeite	4.2	2.2	2.0	6.0	3.8	2.2	7.2
quartz	4.2	2.2	2.0	6.0	3.8	2.2	7.2
feldspar	2.3	1.2	1.1	3.3	2.1	1.2	4.0
feldspar	3.1	1.7	1.4	4.4	2.8	1.6	5.3
Setup Parameters							
Pulse duration τ= 8 ns	Repetition rate = 10 Hz		Total ablation time = 120 s	ϕ_{ω} = 460 μm		$\phi_{2\omega}$ = 380 μm	

Table 1: Parameters used during the laser ablation experiments of the minerals. The pulses have a temporal duration τ = 8 ns. If not otherwise specified, the laser repetition rate was kept at a fixed value of 10 Hz and each sample was irradiated for a total time of 120 s, receiving the total amount of energy E_{total} (last column). In the bottom line, we report parameters that were kept constant across laser ablation experiments (ϕ indicates the diameter of the pulses at the surface of the target). The fluence F_{pulse} and energy E_{pulse} of the laser pulses are the sum of the value at the ω and 2ω frequency of the Nd:YAG laser source. All fluencies and energies used in the current experiments are reported for each mineral ablated, in air (exp. Scenario #1) and in water (exp. Scenario #2).

2.3 Surface profile of the craters formed by laser ablation

After laser ablation, the diameter and depth of each crater (10 total) was measured using a Dektak XT profilometer (Bruker). The DektakXT profilometer is an instrument for determining the surface profile (height and depth) of the chosen sample. It performs surface profile measurements by moving a diamond-tipped needle over the sample surface. The diamond-tipped needle is coupled to a Linear Variable Differential Transformer (LDVT) which produces and processes electrical signals that correspond to surface variations of the sample. Once converted to the digital format, these surface variations are stored for viewing and analysis. The DektakXT profilometer works with the Vision64 measurement and analysis software. This software can optimize system lighting, make single or automated scans, apply filters, and perform special operations such as comparing the analytical results of multiple scans. It also analyzes the aquired

data by applying user-selected analytical functions to estimate the surface texture of the surface sample and other parameters.

We obtained 3D surface maps of the minerals used in our experiments, with special focus on the 3D shape of the craters formed by laser ablation. We worked with 8 nm resolution and “Hills and Valleys” profile-type (this option is typically used when the slope of the surface is unknown or when the sample surface is uneven). We selected a scanned area of 1.0 x 1.5 mm^2. The profilometer images were then analyzed with the Gwyddion program (http://gwyddion.net) to estimate the depth ΔZ and the diameter D of the craters formed by laser ablation. Depth measurements were performed using the extract profile tool. We used a vertical line to select the section of the crater to which the profilometric analysis was applied. This way, we selected two diametrically opposite points at the edge of the crater (indicating the beginning and end of the crater) and calculated the average height of them, which is $\Delta h = (h_1 + h_2) / 2$, where $h_1 = y_{max}$ of the first peak and $h_2 = y_{max}$ of the second peak. We can therefore calculate the depth of the crater, $\Delta Z = \Delta h - y_{min}$, where y_{min} refers to the deepest point inside the crater. The profile analysis described here was applied in five neighboring sections around the crater minimum point. This was done to analyze a larger portion of the crater and try to reduce errors due to morphological irregularities inside the analyzed crater. The same procedure was then repeated by choosing five straight horizontal lines and measuring the depth of the crater also in the horizontal direction. This was done to take into account potential morphological asymmetries of the craters. The crater diameter is measured automatically by the software, when two points are chosen at the edge of the crater.

3. Results and Discussion

For each mineral sample considered in this study (feldspar, quartz and jadeite) 3D surface maps of the craters created by laser ablation were obtained and their average depths and diameters estimated as described in Section 2.3. To increase the number of experimental data, two laser fluences have been considered for each mineral, except for quartz (only one fluence in this case because of a problem with the laser setup during the experimental run). Also, as already mentioned in Section 2.1, two micrometeorite impact scenarios have been simulated for each mineral: ablation in air **and** in water. This way, a total of 10 irradiation experiments were considered (see Table 2). Examples of 3D surface maps of craters formed by laser ablation are shown in Figures 2-4. Blue regions represent depressions in the surface while red regions represent elevetions. Red circles indicate crater locations. These figures show that craters formed in air (**right panel** of Figs 2 - 4) have better-defined boundaries than craters formed in water (**left panel** of Figs 2 - 4). We think that this could be due to a number of phenomena induced by laser heating and ablation at the liquid–solid interface, such as convective bubble motion, explosive boiling, pressure gradients and spurious currents generated within the liquid by the ejected material. These phenomena may play a role in eroding the borders of the craters, limiting the mobility of the ejected material suspended into water and redepositing ejected material onto the surface, resulting in less defined crater boundaries compared to those observed for the ablation experiments performed in air (e.g., Bashir et al. 2013).

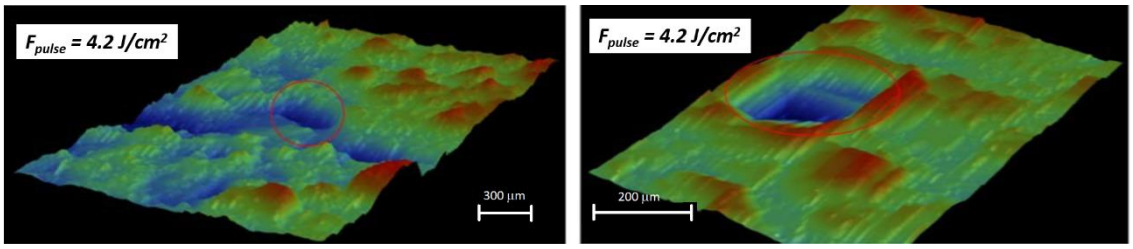

Figure 2: Crater created in the jadeite sample after ablation (1200 total pulses) in deionized H_2O with fluence 4.2 J/cm^2 (left) and after ablation in air with fluence 4.2 J/cm^2 (right). Red circles indicate crater locations.

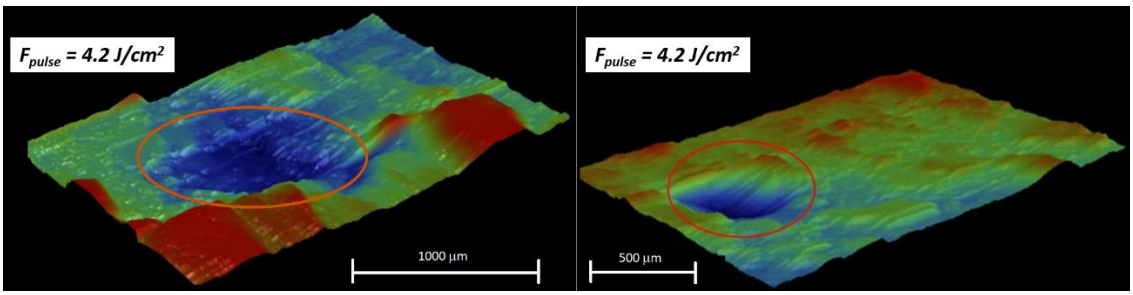

Figure 3: Crater created in the quartz sample after ablation (1200 total pulses) in deionized H_2O with fluence 4.2 J/cm^2 (left) and after ablation in air with fluence 4.2 J/cm^2 (right). Red circles indicate crater locations.

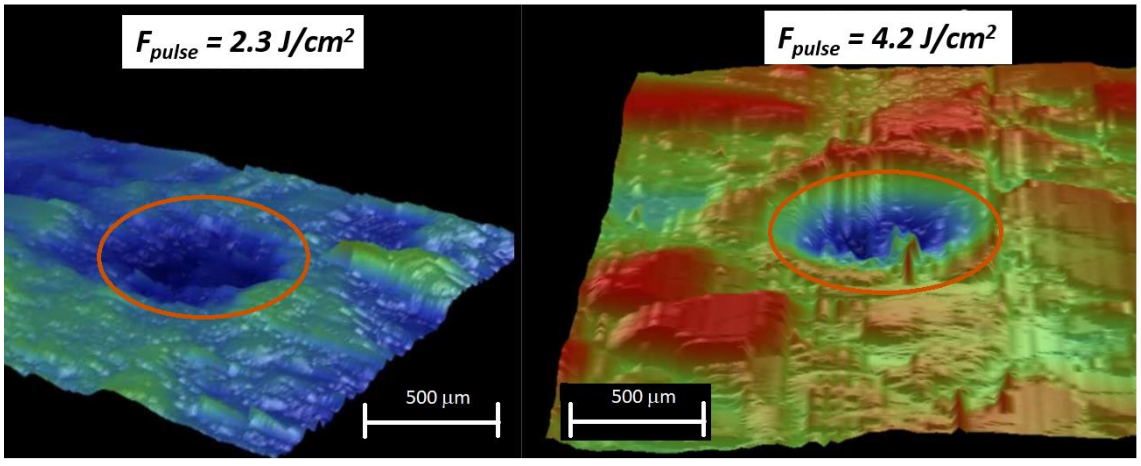

Figure 4: Crater created in the feldspar sample after ablation (1200 total pulses) in deionized H_2O with fluence 2.3 J/cm^2 (left) and after ablation in air with fluence 4.2 J/cm^2 (right). Red circles indicate crater locations.

Mineral	F_{pulse} (J/cm^2)	Average depth ΔZ - μm (RSD)	Average diameter D - μm (RSD)	ΔZ:D
Exp. Scenario #1: air				
jadeite	2.7	128 (26%)	225 (20%)	1:1.8
jadeite	4.2	95 (24%)	179 (23%)	1:1.9
quartz	4.2	258 (11%)	461 (11%)	1:1.8
feldspar	3.8	168 (15%)	369 (23%)	1:2.2
feldspar	4.2	309 (13%)	468 (11%)	1:1.5
ΔZ:D mean value				1:1.8
Exp. Scenario #2: water				
jadeite	2.3	101 (22%)	194 (22%)	1:1.9
jadeite	4.2	95 (15%)	296 (39%)	1:3.1
quartz	4.2	271 (30%)	938 (14%)	1:3.5
feldspar	2.3	146 (41%)	506 (13%)	1:3.5
feldspar	3.1	104 (16%)	626 (13%)	1:6
ΔZ:D mean value				1:2.8*

*does not include the value for the experiment on feldspar with 3.1 J/cm^2

Table 2: Average depth ΔZ and diameter D of the craters formed by laser ablation. Relative standard deviations (RSD) are also reported in parenthesis. Two laser fluences have been considered for each mineral, except for quartz. Two micrometeorite impact scenarios have been simulated for each mineral: ablation in air and ablation in water. The last column shows the value of the ratio ΔZ:D for each of the 10 craters created by laser ablation.

The main result of our analysis revolves around depth:diameter ratios (ΔZ:D) – a primary parameter for characterizing impact craters. The last column of Table 2 shows the value of ΔZ:D for each crater, in each experimental scenario considered. In planetary science, impact craters may be classified in two main groups depending on their morphology: complex or simple craters. Complex impact craters are relatively large and typically exhibit a central peak with terraced (i.e., stepped) walls. The typical depth:diameter ratio for complex craters peaks in the range from 1:10 to 1:20 (i.e., 0.1 – 0.05). On the other hand, simple impact craters are relatively small and they are characterized by bowl-shaped depressions with mostly smooth walls. The typical depth:diameter ratio for simple craters peaks in the range from 1:4 to 1:10 (i.e., 0.25 – 0.1). The diameter at which the transition from simple to complex crater occurs depends on the planetary body under consideration and, in particular, on its surface gravity. For example, on Earth the transition from simple to complex crater occurs for diameters above 2 to 4 km, depending on the properties of the rocky target. On the Moon, this transition occurs above 15 to 20 km. On asteroid (4) Vesta occurs above 30 to 35 km. These and additional information on complex and simple craters may be found elsewhere in the literature (e.g., Koeberl and Sharpton, LPI website; Melosh 1989; Pilkington and Grieve, 1992; Vincent et al. 2014, Stopar et al., 2017; Robbins et al., 2018; and references therein). Although micrometeorite craters morphologically resemble simple craters, their typical depth:diameter ratio is a bit different from the values mentioned above. For micrometeorite craters its value peaks in the range from 1:1.4 to 1:3.5 (i.e., 0.71 – 0.29), with a mean value equal to 1:1.9 (i.e., 0.53) (Love and Brownlee 1993). These values were determined from the analysis of impact craters created by micrometeoroids (mass range: 10^{-9} - 10^{-4} grams) on the space-facing end of NASA Long Duration Exposure Facility, operating at altitudes among 331 and 480 km.

A total of 761 craters were found on the 5.6 m^2 panels of the satellite exposed over a period of 5.77 years. A subset of 609 impact craters were selected and their diameters and depths were measured using a Zeiss GFL compound microscope and a Wildt stereo microscope. Using these measurements, the aforementioned depth:diameter ratio range was determined for micrometeorite impact craters (details can be found in Love and Brownlee 1993).

Depth:diameter ratios from this study (last column of Table 2) are largely consistent with those reported in the literature, with the depth:diameter ratios ranging from 1:1.5 to 1:3.5 (i.e., 0.67 – 0.29) in 9 out of 10 experiments. Moreover, the mean value for the experiments performed in air is 1:1.8 (i.e., 0.56), again, in good agreement with literature values. The mean value for the experiments performed in water is slightly **lower**, 1:2.8 (i.e., 0.36). The outstanding agreement with the literature data clearly indicates that the simple craters produced in our laser ablation setup, especially in air, closely resemble the morphology of natural micrometeorite craters. The only exception occurs for the feldspar sample irradiated in water with a high fluence, whose depth:diameter ratio of 1:6 (i.e., 0.17) lies outside the range of values **cited in the literature (as discussed above)**. Nevertheless, Love and Brownlee (1993) showed that there is a small (but not zero) probability to find depth:diameter ratio values above 1:3.5 (i.e., below 0.29), their number decreasing to zero when moving toward the limit ratio value of 1:10 (i.e., 0.1). This information makes us believe that the feldspar data showing a ratio value equal to 1:6 is genuine although we cannot explain why it is significantly different from the other values.

In addition, when comparing the results of the experiments in air (ranging from 0.67 to 0.45, with mean value of about 0.56) with those in water (ranging from 0.53 to 0.29, with mean value of about 0.36) looks like depth:diameter ratios are slightly

shifted. This suggest that the depth:diameter ratio could be related to the medium in which the impacts occur or, in other words, to the phenomena induced by impact heating and ablation at the liquid–solid interface, such as convective bubble motion, explosive boiling, pressure gradients and spurious currents generated within the liquid by the material ejected (i.e., Bashir et al. 2013). Results listed in Table 2 highlight this slight morphological difference between our laser ablation experiments performed in air and in water, however, we believe that our current experimental set (10 experiments total) is too limited to investigate this difference further. **Additional experiments, including repetitions of the experiments carried out in the present study, are needed to perform a robust statistical analysis of morphological results.** Our goal is to generate a comprehensive dataset on the morphology of craters created by laser ablation of various minerals relevant to planetary science.

Finally, we want to point out that although micrometeorite impacts consist of one single event, within errors, the main parameter characterizing the impact craters created by laser ablation, i.e. the depth:diameter ratio (ΔZ:D), does not show a strong dependence on the total fluence received after n pulses but only depends on $\boldsymbol{F_{pulse}}$ (J/cm^2), the fluence associated to each pulse (see Table 1). All experimental data discussed so far were produced from laser ablation experiments employing the same laser repetition frequency (10 Hz) and irradiation time (120 sec), resulting in 1200 pulses total per ablation experiment. These parameters ensure craters with well-defined boarders form, thus facilitating their morphological characterization. To verify that the depth:diameter ratio (ΔZ:D) does not depend on the total fluence received after n pulses but only on the fluence of each pulse, we have performed additional laser irradiation experiments on the same jadeite sample in air (irradiating each time a different spot of its surface) and comparing the craters formed with 1, 10, 100 and 1200 total pulses,

keeping fixed $\boldsymbol{E_{pulse}}$ = 6 mJ and $\boldsymbol{F_{pulse}}$ = 4.2 J/cm^2 (the laser repetition frequency for the craters formed with 1, 10, and 100 pulses was set equal to 1 Hz). When comparing these impact craters the value of the depth:diameter ratio ranges from 1:1.88 to 1:2.7 (i.e., 0.53 – 0.37), with an average value of about 1:2.3 (i.e., 0.43). From Figure 5 it appears that, within errors, the depth:diameter ratio does not seem to depend on the total number of laser pulses **or** the laser repetition frequency used during the irradiation experiments (see also Table 3). This can be said at least for the experimental ranges here covered: i) between 1 and 1200 laser pulses and ii) between 1 and 10 Hz.

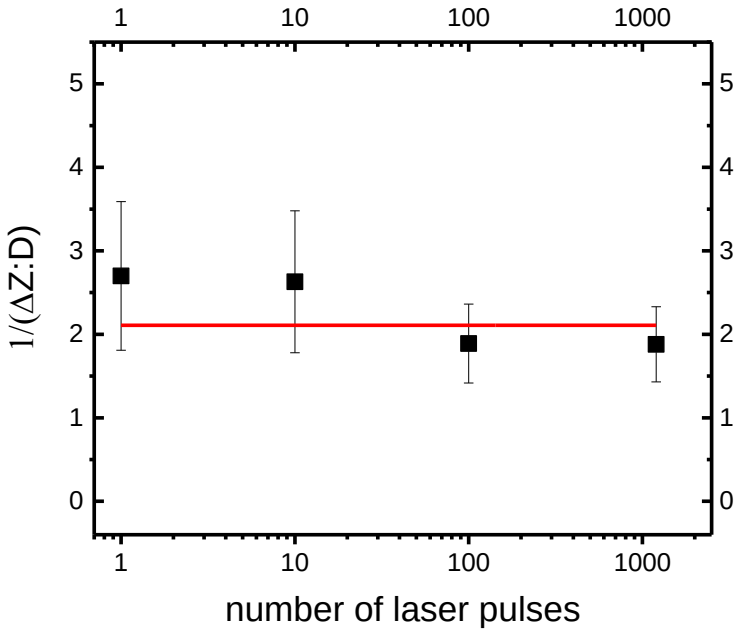

Figure 5: Reciprocal of the depth:diameter ratio for the impact craters formed in air on the jadeite sample as a function of the total number of laser pulses: 1, 10, 100, and 1200 pulses. For all experiments $\boldsymbol{E_{pulse}}$ and $\boldsymbol{F_{pulse}}$ have been kept fixed and equal to 6 mJ and 4.2 J/cm^2, respectively. To guide the reader's eye, the intercept y=2.1 (discretionally chosen) is shown as a red line.

N. pulses	Average depth ΔZ - μm (RSD)	Average diameter D - μm (RSD)	ΔZ:D
jadeite in air			
1	88 (32%)	238 (32%)	1:2.7
10	53 (33%)	138 (33%)	1:2.6
100	112 (22%)	218 (24%)	1:1.9
1200	95 (24%)	179 (23%)	1:1.9

Table 3: Average depth ΔZ, diameter D, and ratio ΔZ:D for for the impact craters formed in air on the jadeite sample as a function of the total number of laser pulses: 1, 10, 100, and 1200 pulses. For all experiments $\boldsymbol{E_{pulse}}$ and $\boldsymbol{F_{pulse}}$ have been kept fixed and equal to 6 mJ and 4.2 J/cm^2, respectively. Relative standard deviations (RSD) are also reported in parenthesis.

4. Conclusions

In this work, we have studied the ability of ns-pulsed laser ablation to appropriately simulate the morphology of natural micrometeorite impact craters on airless bodies. We applied the laser ablation technique to three different silicate samples, jadeite, quartz and feldspar, representing important minerals of great interest in the field of terrestrial and planetary science. For each silicate sample two ablation scenarios have been considered: in air and in water. The surface profile of the craters formed by ns-pulsed laser ablation was analyzed by profilometry and for each crater the average depth, diameter, and depth:diameter ratio (ΔZ:D) was estimated. By comparing our experimental results with literature data, we conclude that the simple craters formed by ns-pulsed laser ablation closely resemble impact craters formed by micrometeorite impacts. In particular, we point out that the depth:diameter ratio found in 9 out of 10 experiments ranges from 1:1.5 to 1:3.5 (i.e., 0.67 – 0.29), with a mean value for the

experiments performed in air equals to 1:1.8 (i.e., 0.56). For micrometeorite craters, literature data indicate that ΔZ:D ranges from 1:1.4 to 1:3.5 (i.e., 0.71 – 0.29), with a mean value equal to 1:1.9 (i.e., 0.53) (Love and Brownlee 1993). In other words, from a morphological point of view the experimental method discussed here, ns-pulsed laser ablation, is appropriate for the simulation of micrometeorite impacts.

By performing additional ablation experiments on jadeite in air with 1, 10, 100, and 1200 pulses, we also verified that crater depth:diameter ratios do not depend, within errors, on the total number of laser pulses or the repetition frequency, at least for the experimental ranges here covered, i.e., i) between 1 and 1200 laser pulses and ii) between 1 and 10 Hz. Such a result is important because it proves that, within these experimental conditions, the depth:diameter ratio of craters produced by ns-pulsed laser ablation depends only on the fluence of the incident laser pulse (F_{pulse}). The implication of this finding is that one can perform experiments with n>1 laser pulses to create craters with well-defined boarders, thus facilitating their morphological characterization. In detail, the value of the depth:diameter ratio was found to range from 1:1.88 to 1:2.7 (i.e., 0.53 – 0.37), with an average value of about 1:2.3 (i.e., 0.43).

As far as we know, the present work is the first one dedicated to the morphological characterization of impact craters created by ns-pulsed laser ablation and showing that ns-pulsed lasers can be employed to simulate and study, from a morphological point of view, micrometeorite impact craters on the surface of asteroids, comets, and some planets and their satellites. The present study should be considered as a starting point in this exciting field of research and additional experiments on feldspar, jadeite, and quartz mineral samples are needed to improve statistical analyses. Additional experiments are also desirable to verify, for other minerals, that the depth:diameter ratio only depends on $\boldsymbol{F_{pulse}}$ thus extending the results here discussed for

jadeite. The long-term goal is to generate a comprehensive dataset on the morphology of craters created by laser ablation of various minerals relevant to planetary science.

Acknowledgment

Authors thank the Brazilian Agencies FAPERJ, CNPq and CAPES for financial support and fellowships. Authors gratefully acknowledge Dr. C. R. Ponciano for providing us the mineral samples and Profs. Cremona, Lazaro, and Maia da Costa at the Physics Dept. of PUC-Rio for the use of the equipment and infrastructure.

References:

- Amendola, V. and Meneghetti, M. 2013, Physical Chemistry Chemical Physics, 15, 3027-3046; https://doi.org/10.1039/C2CP42895D

- Anderson, R. S., and Anderson, S., P., 2010, Geomorphology: The Mechanics and Chemistry of Landscapes. Cambridge University Press.; https://doi.org/10.1017/S0016756810000932

- Araujo, J. F. D. F. et al. 2020, Journal of Magnetism and Magnetic Materials, 499, 166300; https://doi.org/10.1016/j.jmmm.2019.166300

- Babushok, V. I., DeLucia, F. C., Gottfried, J. L., Munson, C. A. and Miziolek, A. W., 2006, Spetrochimica Acta B, 61, 999; https://doi.org/10.1016/j.sab.2006.09.003

- Barnouin, O. S., Terik Daly, R., Cintala, M. J., Crawford, D. A., 2019, Icarus, 325, 67; https://doi.org/10.1016/j.icarus.2019.02.004

622 - Bashir, S., Vaheed, H. and Mahmood, K. 2013, Appl. Phys. A, 110, 389;
623 https://doi.org/10.1007/s00339-012-7175-0

624 - Bockelée-Morvan, D., Rinaldi, G., Erard, S., et al. 2017, MNRAS, 469, S443;
625 https://doi.org/10.1093/mnras/stx1950

626 - Born, M. and Wolf, E. 1999, Principles of Optics, 7th edition, Cambridge University
627 Press, ISBN 9781139644181; https://doi.org/10.1017/CBO9781139644181

628 - Brunetto, R. and Strazzulla, G., 2005, Icarus, 179, 265-273;
629 https://doi.org/10.1016/j.icarus.2005.07.001

630 -Brunetto, R., Romano, F., Blanco, A., Fonti, S., Martino, M., 2006, Icarus, 180, 546;
631 https://doi.org/10.1016/j.icarus.2005.10.016

632 - Brunetto, R., Loeffler, M. J., Nesvorný, D., Sasaki, S., Strazzulla, G., 2015, Asteroids
633 IV, University of Arizona Press, Tucson, 597;

634 - Cabalin, L. M. and Laserna, J. J. 1998, Spectroquimica Acta Part B, 53, 723-730;
635 https://doi.org/10.1016/S0584-8547(98)00107-4

636 - Cassata, W. S., Cohen, B. E., Mark, D. F., Trappitsch, R., Crow, C. A., Wimpenny, J.,
637 Lee, M. R., Smith, C. L. 2018, Science Advances, 4, eaap8306;
638 https://doi.org/10.1126/sciadv.aap8306

639 - Cassidy, W., and Hapke, B., 1975, Icarus, 25, 371; https://doi.org/10.1016/0019-
640 1035(75)90002-0

641 - Chapman C. R., 2004, Annual Review of Earth and Planetary Sciences, 32, 539;
642 https://doi.org/10.1146/annurev.earth.32.101802.120453

- Cheung, J. and Horwitz, J. 1992, MRS Bulletin, 17(2), 30-36; https://doi.org/10.1557/S0883769400040598

- Christoffersen, R., Loeffler, M. J., Dukes, C. A., Keller, L. P., Baragiola, R. A., 2016, 47th Lunar and Planetary Science Conference, held March 21-25, 2016 at The Woodlands, Texas. LPI Contribution No. 1903, p.2747

- Cintala, M. J., Berthoud, L. and Horz, F. 1999, Meteoritics & Planetary Science, 34, 605; https://doi.org/10.1111/j.1945-5100.1999.tb01367.x

- Clark, B. E., Hapke, B., Pieters, C., Britt, D., 2002, Asteroids III, University of Arizona Press, Tucson, 585;

- Del Rosso, T., et al. 2016, Nanotechnology, 27(25):255602; https://doi.org/10.1088/0957-4484/27/25/255602

- Del Rosso, T., et al. 2018, Applied Surface Science, 441, 347; https://doi.org/10.1016/j.apsusc.2018.02.007

- Dou, H., Yao, C., Liu, H., Wan, Y., Ding, R., Yuan, X., and Xu, S., 2018, Applied Surface Science, 447, 388; https://doi.org/10.1016/j.apsusc.2018.04.003

- Dyar, M. D., Delaney, J. S. and Tegner, C. 2001, LPSC XXXII, #1065;

- Fulvio, D., Perna, D., Ieva, S., Brunetto, R., Kanuchova, Z., Blanco, C., Strazzulla, G., Dotto, E., 2016, MNRAS, 455, 584; https://doi.org/10.1093/mnras/stv2300

- Fulvio, D., Ieva, S., Perna, D., Kanuchova, Z., Mazzotta Epifani, E., Dotto, E., 2018, Planetary and Space Science, 164, p. 37; https://doi.org/10.1016/j.pss.2018.06.006

- Gaffey, M. J., 2010, Icarus, 209, 564; https://doi.org/10.1016/j.icarus.2010.05.006

- Ganeev, R. A., Chakravarty, U., Naik, P. A., Srivastava, H., Mukherjee, C., Tiwari, M. K., Nandedkar, R. V., Gupta, P. D. 2007, Applied Optics, 46, 1205-1210; https://doi.org/10.1364/AO.46.001205

- Gillis-Davis, J. J., Lucey, P. G., Bradley, J. P., Ishii, H. A., Kaluna, H. M. Misra, A., Connolly Jr., H. C. 2017, Icarus, 286, 1; https://doi.org/10.1016/j.icarus.2016.12.031

- Giorgetti, E., Giusti, A., Giammanco, F., Laza, S., Del Rosso, T., Dellepiane, G. 2007, Applied Surface Science, 254, 1140-1144; https://doi.org/10.1016/j.apsusc.2007.09.057

- Greer, J., Rout, S. S., Isheim, D., Seidman, D. N., Wieler, R., Heck, P. R. 2020, Meteoritics and Planetary Science, 55, 426-440; https://doi.org/10.1111/maps.13443

- Grün, E., Zook, H. A., Fechtig, H., Giese, R. H. 1985, Icarus, 62, 244; https://doi.org/10.1016/0019-1035(85)90121-6

- Gusarov, A. V. and Smurov, I. 2005, Journal of Applied Physics, 97, 014307; https://doi.org/10.1063/1.1827321

- Hapke, B., 2001, Journal of Geophysical Research: Planets, 106, 10039; https://doi.org/10.1029/2000JE001338

- Harlow, G. E. and Shi, G., 2011, Gems and Gemology, XLVII, 116-117;

- Hashida, M., Mishima, H., Tokita, S., Sakabe, S. 2009, Optics Express, 17, 13116-13121; https://doi.org/10.1364/OE.17.013116

- Hill, L., C. 2016, Mineralogical Inventories of all 62 HED meteorite Falls, https://www.mindat.org/article.php/2115;

- Hofmeister, A., M and Rossman, G., R. 1984, Phy Chem Minerals, 11, 213-224; https://doi.org/10.1007/BF00308136

- Jaeggi, B., Neuenschwander, B., Schmid, M., Muralt, M., Zuercher, J., Hunziker, U. 2011, Physics Procedia, 12, B, 164-171; https://doi.org/10.1016/j.phpro.2011.03.118

- Kaluna, H. M., Ishii, H. A., Bradley, J. P., Gillis-Davis, J. J., Lucey, P. G. 2017, Icarus, 292, 245; https://doi.org/10.1016/j.icarus.2016.12.028

- Kimura M., Weisberg M. K., Lin Y., Suzuki A., Ohtani E., Okazaki R. 2005. Meteoritics and Planetary Science, 40, 855–868; https://doi.org/10.1111/j.1945-5100.2005.tb00159.x

- Kissel, J., and Krueger, F. R., 1987, Applied Physics A, 42, 69; https://doi.org/10.1007/BF00618161

- Koeberl, C., and Sharpton, V. L., Terrestrial Impact Craters Slide Set, Lunar and Planetary Institute: https://www.lpi.usra.edu/publications/slidesets/craters/

- Kohout, T., Penttila, A., Mann, P., Cloutis, E., Cuda, J., Filip, J., Malina, O., Reddy, V., Grokhovsky, V., Yakovlev, A., Halodova, P., Haloda, J., 2020, The Planetary Science Journal, 1, 37; https://doi.org/10.3847/PSJ/aba7c2

- Komatsu, M., Fagan, T. J., Krot, A. N., Nagashima, K., Petaev, M. I., Kimura, M., and Yamaguchi, A. 2018, PNAS, 115, 29, 7497; https://doi.org/10.1073/pnas.1722265115

- Lide, D. R., 2004. Handbook of Chemistry and Physics 85th Edition, Editor in Chief Lide, D. R., CRC Press, Boca Raton, Florida, ISBN 0-8493-0485-7

- Liu, X., Du, D., Mourou, G. 1997, IEEE Journal of Quantum Electronics, 33, 1706-1716; https://doi.org/10.1109/3.631270

- Loeffler, M.J., Baragiola, R.A., Murayama, M., 2008, Icarus 196, 285; https://doi.org/10.1016/j.icarus.2008.02.021

- Loeffler, M. J., Dukes, C. A., and Baragiola, R. A., 2009, Journal Geophysical Research – Planets, 114, 3003; https://doi.org/10.1029/2008JE003249

- Love, S. G. and Brownlee, D. E., 1993, Science, 262, 550; https://doi.org/10.1126/science.262.5133.550

- Ma, C., Tschauner, O., Beckett, J. R., Liu, Y., Rossman, G. R., Zhuravlev, K., Prakapenka, V., Dera, P. Taylor, L., A., 2015, Earth and Planetary Science Letters, 422, 194-205; https://doi.org/10.1016/j.epsl.2015.03.057

- Matsumoto, T., et al., 2016, Geochimica et Cosmochimica Acta, 187, 195-217; https://doi.org/10.1016/j.gca.2016.05.011

- Matsumoto, T., Harries, D., Langenhorst, F., Miyake, A. and Noguschi, T., 2020, Nature Communications, 11, 1117; https://doi.org/10.1038/s41467-020-14758-3

- Matsuoka, M., Nakamura, T., Kimura, Y., Hiroi, T., Nakamura, R., Okumura, S. and Sasaki, S. 2015, Icarus, 254, 135; https://doi.org/10.1016/j.icarus.2015.02.029

- Melosh, H.J. 1989. Impact Cratering: A Geologic Process. Oxford University Press, U.K.

- Miyahara, M., Ohtani, E. and Yamaguchi, A. (2015) High–pressure polymorphs in Gujba CB type carbonaceous chondrite. 2015 Japan Geoscience Union Meeting, PPS22–20;

- Moroz, L. V., Fisenko, A. V., Semjonova, L. F., Pieters, C. M., and Korotaeva, N. N. 1996, Icarus, 122, 366; https://doi.org/10.1006/icar.1996.0130

- Nassau, K. and Shigley, J. E. 1987, Gems and Gemology, XXIII, 27-35;

- Noble, S. K., Keller, L. P., Christoffersen, R., Rahman, Z., 2016, 47th Lunar and Planetary Science Conference, held March 21-25, 2016 at The Woodlands, Texas. LPI Contribution No. 1903, p.1465

- Noguchi, T. et al., 2014, Meteoritics and Planetary Science, 49, 188–214; https://doi.org/10.1111/maps.12111

- Norton, O. R. and Chitwood, L., 2008, Field Guide to Meteors and Meteorites, Springer

- Ohtani, E. Ozawa, S., Miyahara, M. 2017, Journal of Mineralogical and Petrological Sciences, 112, 247-255; https://doi.org/10.2465/jmps.170329

- Ootsubo, T., Kawakita, H., Shinnaka, Y., Watanabe, J., and Honda, M. 2020, Icarus, 338, 113450; https://doi.org/10.1016/j.icarus.2019.113450

- Ozawa, S., Miyahara, M., Ohtani, E., Koroleva, O., Ito, Y., Litasov, K., Pokhilenko, N. 2014, Scientific Reports, 4, 5033; https://doi.org/10.1038/srep05033

- Pang, R-L., Zhang, A-C., Wang, S-Z., Wang, R-C., Yurimoto, H. 2016, Scientific Reports, 6, 26063; https://doi.org/10.1038/srep26063

- Perez, D. and Lewis, L. J. 2003, Phys. Rev. B, 67, 184102; https://doi.org/10.1103/PhysRevB.67.184102

- Pieters, C.M., Taylor, L.A., Noble, S.K., Keller, L.P., Hapke, B., Morris, R.V., Allen, C.C., McKay, D.S., Wentworth, S., 2000, Meteorititics and Planetary Science, 35, 1101-1107; https://doi.org/10.1111/j.1945-5100.2000.tb01496.x

- Pieters, C. M. & Noble S. K., 2016, Journal of Geophysical Research: Planets, 121, 1865; https://doi.org/10.1002/2016JE005128

751 - Pilkington, M. and Grieve, R. A. F., Reviews of Geophysics, 1992, vol. 30, pp. 161;
752 https://doi.org/10.1029/92RG00192

753 - Plane, J. M. C., Flynn, G. J., Määttänen, A., Moores, J. E., Poppe, A. R., Carrillo-
754 Sanchez, J. D., Listowski C. 2018, Space Science Review, 214, 23;
755 https://doi.org/10.1007/s11214-017-0458-1

756 - Polyak, D. E., Dyar, M. D., Delaney, J. S. and Tegnar, C. 1999, LPSC XXX, #1911;

757 - Prince, B. S., Magnuson, M. P., Chaves, L. C., Thompson, M. S., Loeffler, M. J. 2020,
758 Journal of Geophysical Reseach: Planets, 125, e2019JE006242;
759 https://doi.org/10.1029/2019JE006242

760 - Radziemski, L. J., 1994, Microchemical Journal, 50, 218;
761 https://doi.org/10.1006/mchj.1994.1090

762 - Robbins, S., J., Watters, W., A., Chappelow, J. E., Bray, V., Daubar, I., J., Craddock,
763 R. A., Beyer, R., A., Landis, M., ostrach, L., R., Tornabene, L., Riggs, J. D., Weaver,
764 B., P. 2018, Meteoritics and Planetary Science, 53, 583;
765 https://doi.org/10.1111/maps.12956

766 - Rossman, G. 1974, American Mineralogist, 59, 868-870;

767 - Rudnick, R. L., and Gao, S., 2003, Composition of the Continental Crust, In Holland,
768 H. D. and Turekian, K. K. (eds.), Treatise on Geochemistry. 3, New York: Elsevier
769 Science, pp. 1–64;

770 - Sasaki, S., Nakamura, K., Hamabe, Y., Kurahashi, E., and Hiroi, T., 2001, Nature,
771 410, 555; https://doi.org/10.1038/35069013

772 - Sasaki, S., Kurahashi, E., Nakamura, K., Yamanaka, C., 2002, Earth, Planets and
773 Space, 54, e5-e7;

- Scharf, T. and Krebs, H. 2002, Appl. Phys. A, 75, 551–554; https://doi.org/10.1007/s00339-002-1442-4

- Shinno, I. and Oba, T. 1993, Mineralogica Journal, 16, 378-386; https://doi.org/10.2465/minerj.16.378

- Shu, A., Collette, A., Drake, K., Grun, E., Horanyi, M. et al. 2012, Review of Scientific Instruments, 83, 075108; https://doi.org/10.1063/1.4732820

- Sikora, A., Grojo, D., Sentis, M., 2017, Journal of Applied Physics, 122, 045702; https://doi.org/10.1063/1.4994307

- Stopar, J. D., Robinson, M. S., Barnouin, O., S., McEwen, A. S., Speyerer, E. J., Henriksen, M. R., Sutton, S. 2017, Icarus, 298, 34; http://dx.doi.org/10.1016/j.icarus.2017.05.022

- Szurgot, M. 2014, Vesta in the Light of Dawn: First Exploration of a Protoplanet in the Asteroid Belt, held 3-4 February, 2014 in Houston, Texas. LPI Contribution No. 1773, p.2052;

- Thomas, E., Horanyi, M., Janches, D., Munsat, T., Simolka, J., Sternovsky, Z., 2016, Geophysical Research Letters, 43, 3645; https://doi.org/10.1002/2016GL068854

- Thomas, E., Simolka, J., DeLuca, M., Horanyi, M., Janches, D., Marshall, R. A., Munsat, T., Plane, J. M. C., Sternovsky, Z., 2017, Review of Scientific Instruments, 88, 034501; https://doi.org/10.1063/1.4977832

- Thompson, M. S., Loeffler, M. J., Morris, R. V., Keller, L. P., Christoffersen, R. 2019, Icarus, 319, 499; https://doi.org/10.1016/j.icarus.2018.09.022

- Thompson, M. S., Morris, R. V., Clemett, S. J., Loeffler, M. J., Trang, D., Keller, L. P., Christoffersen, R., Agresti, D. G. 2020, Icarus, 356, 113775; https://doi.org/10.1016/j.icarus.2020.113775

- Tomioka, N. and Miyahara, M. 2017, Meteoritics and Planetary Science, 52, 9, 2017–2039; https://doi.org/10.1111/maps.12902

- Vanzani, V., Marzari, F., Dotto, E., 1997, Lunar and Plan. Sci. Conf., 28, 1481

- Vincent, J., -B, Schenk, P., Nathues, A., et al. 2014, Planetary and Space Science, 103, 57; https://doi.org/10.1016/j.pss.2013.09.003

- Wasson, J. T.; Pieters, C. M.; Fisenko, A. V.; Semjonova, L. F.; Warren, P. H.,1998, 29th Annual Lunar and Planetary Science Conference, March 16-20, 1998, Houston, TX, abstract no. 1940;

- Weber, I., Stojic, A. N., Morlok, A., Reitze, M. P., Markus, K., Hiesinger, H., Pavlov, S. G., Wirth, R., Scheiber, A., Sohn, M., Hubers, H.-W., Helbert, J., 2020, Earth and Planetary Science Letters, 530, 115884; https://doi.org/10.1016/j.epsl.2019.115884

- Wu, Y., Li, X., Yao, W., and Wang, S., 2017, Journal of Geophysical Research: Planets, 122, 1956; https://doi.org/10.1002/2016JE005220

- Yamada, M., Sasaki, S, Nagahara, H., Fujiwara, A., Hasegawa, S., Yano, H., Hiroi, T., Ohashi, H., and Otake, H., 1999, Earth Planets Space, 51, 1255; https://doi.org/10.1186/BF03351599

- Yurij, C. and Vekhov, A., 1979, Journal of Physics D: Applied Physics, 12, 539-553; https://doi.org/10.1088/0022-3727/12/4/011

- Zhang, A., Kawasaki, N., Bao, H., Liu, J., Qui, L., Kuroda, M., Gao, J-F.,C. L.H., He, Y., Sakamoto, N., Yurimoto, H. 2020, Nature Communications, 11, 1289; https://doi.org/10.1038/s41467-020-15049-7

- Zheng, B., Jiang, G., Wang, W., Wang, K., Mei, X. 2014, AIP Advances, 4, 031310; https://doi.org/10.1063/1.4867088

- Zolensky, M., Bland, P., Brown, P., and Halliday, I., 2006, Meteorites and the Early Solar System II, D. S. Lauretta and H. Y. McSween Jr. (eds.), University of Arizona Press, Tucson, 943, 869-888.

- Xu, S., Yao, C., Liao, W., Yuan, X., Wang, T., and Zu, X., 2016, Nuclear Instruments and Methods in Physics Research B, 385, 46; https://doi.org/10.1016/j.nimb.2016.06.016